



## ORIGINAL ARTICLE

# Combustion performance of hybrid rocket fuels loaded with $\text{MgB}_2$ and carbon black additives

Yash Pal<sup>a,\*</sup>, Sasi Kiran Palateerdham<sup>b</sup>, Sri Nithya Mahottamananda<sup>c</sup>,  
Subha Sivakumar<sup>a</sup>, Antonella Ingenito<sup>b</sup>

<sup>a</sup>School of Aeronautical Sciences, Hindustan Institute of Technology and Science, Chennai, 603103, India

<sup>b</sup>School of Aerospace Engineering, University of Rome "La Sapienza", 00138, Rome, Italy

<sup>c</sup>Department of Aerospace Engineering, BS Abdur Rahman Crescent Institute of Science & Technology, Chennai, 600048, India

Received 12 January 2022; accepted 25 August 2022

Available online XXXX

## KEYWORDS

Hybrid rocket;  
Paraffin wax;  
Regression rate;  
Magnesium diboride;  
Mechanical properties

**Abstract** Paraffin-based fuel has a great potential for several innovative missions, including space tourism, due to its safety, low environmental impact, high performance and low cost. Despite the fact that liquefying solid fuels increases the regression rate of hybrid rocket motors, incorporating energetic materials into solid fuel can still improve the performance. The objective and scope of this study is to increase the performance characteristics of the paraffin-based fuel by using magnesium diboride ( $\text{MgB}_2$ ) and carbon black (CB) additives. The cylindrical-port fuel grains were manufactured with various additives percentages in mass (wt%: CB-2% and  $\text{MgB}_2$ -10%) and tested using a laboratory-scale ballistic hybrid motor under gaseous oxygen. The mechanical performance results revealed that adding CB and  $\text{MgB}_2$  improved the ultimate strength and elastic modulus of paraffin-based fuels. The addition of these fillers increased the hardness of fuel by developing a strong interaction in the paraffin matrix. Thermogravimetry (TG) results showed that CB inclusion improved the thermal stability of the paraffin matrix. The average regression rates of fuels loaded with CB and  $\text{MgB}_2$  were 32% and 52% higher than those of unmodified paraffin wax, respectively. The characteristic velocity efficiency was found in the range of 68%–79% at an O/F ratio of 1.5–2.6. The  $\text{MgB}_2$

\*Corresponding author.

E-mail address: [yashpal@hindustanuniv.ac.in](mailto:yashpal@hindustanuniv.ac.in) (Yash Pal).

Peer review under responsibility of Propulsion and Power Research.



Production and Hosting by Elsevier on behalf of KeAi

<https://doi.org/10.1016/j.jprr.2022.11.003>

2212-540X/© 2022 The Authors. Publishing services by Elsevier B.V. on behalf of KeAi Communications Co. Ltd. This is an open access article under the CC BY-NC-ND license (<http://creativecommons.org/licenses/by-nc-nd/4.0/>).

oxidation/combustion in the paraffin matrix was described by a four-step oxidation process ranging from 473 K to 1723 K. Finally, a combustion model of  $MgB_2$  in the paraffin matrix was proposed, and four-step oxidation processes were discussed in detail.

© 2022 The Authors. Publishing services by Elsevier B.V. on behalf of KeAi Communications Co. Ltd.

This is an open access article under the CC BY-NC-ND license (<http://creativecommons.org/licenses/by-nc-nd/4.0/>).

## Nomenclature

$A$	port area (unit: $mm^2$ )
$a$	mass flux exponent
$C^*$	characteristic velocity (unit: m/s)
$d$	diameter (unit: mm)
$G$	mass flux (unit: $kg/(m^2 \cdot s)$ )
$l$	length (unit: mm)
$m$	mass (unit: g)
$\dot{m}$	mass flow rate (unit: kg/s)
$n$	mass flux coefficient
$P$	pressure (unit: $N/m^2$ )
$q$	Rayleigh number
$t$	burn time (unit: s)

## Greek letters

$\eta$	efficiency
$\zeta$	uncertainty

## Subscripts

$b$	burn
$c$	chamber
$exp$	experimental
$f$	fuel
$ig$	ignition
$ox$	oxidiser
$p$	port
$r$	radiation
$theor$	theoretical

## 1. Introduction

Several reports on the space market forecast the potential growth for human spaceflight, space tourism, and small satellite launches. Considering the Northern Sky Research satellite market report, 1000 smallsats/year are required to be launched in the next 10-year period [1]. The traditional solid and liquid rocket launch vehicle capability cannot meet the future satellite market growth [2]. The dedicated hybrid launch vehicles could be a potential solution to meet the future demand for micro/nanosatellite launches. A hybrid launch vehicle can offer several advantages such as low cost, operational safety, controllability, and low environmental impact compared to other counterparts [3]. Despite these unique features, the hybrid propulsion system still has several practical challenges, such as low regression

rate of fuel, low volumetric loading, change in O/F ratio during operation, and low combustion efficiency [4]. The low regression rate of polymer-based fuel is due to diffusion-limited combustion governed by convection and radiation transport rather than chemical kinetics [5].

In recent decades, several researchers have attempted to overcome these drawbacks and improve hybrid propulsion technology. A multiport-fuel-grain design approach was adopted to increase the thrust and low regression rate [6], swirl injection of the oxidiser [3,7,8], and the addition of metal additives and energetic particles [9–11]. Karabeyoglu et al. [12] introduced paraffin-based fuels that can offer 3–4 times higher regression rates than conventional polymer-based fuels. The combustion phenomenon associated with these high regression rate fuels is different from traditional polymeric fuels. During the combustion, paraffin fuel produces an unstable low surface tension liquid layer on the surface of the fuel. When the oxidiser jet passes over the unstable melted layer, it generates fuel droplets from the surface and is entrained into the combustion zone [13]. Therefore, the entrained mass of liquid fuel droplets results in a high fuel regression rate compared to traditional polymeric fuel.

Although paraffin-based fuels showed an effective way to increase the regression rate performance alongside low cost, safety, and environmentally friendly features, they exhibit poor mechanical characteristics [14]. Moreover, the paraffin droplets stripped off the molten liquid layer during the combustion process remain unburned and ejected through the exhaust nozzle. This ultimately results in the low combustion efficiency of paraffin-based fuel compared to usual polymeric fuel. Several studies have been reported to improve the mechanical performance, combustion efficiency, and energy density of paraffin-based fuel. The addition of additives such as low-density polyethylene (LDPE), carbon black (CB), ethylene-vinyl acetate (EVA), and nano metallic additives can significantly improve the mechanical performance and combustion efficiency of paraffin [15–18]. However, adding such additives can diminish the positive effect of paraffin wax as a high regression rate fuel.

Kim et al. [16] tested paraffin-PE blended fuels for mechanical and regression rate performance. The inclusion of PE into paraffin significantly improved the combustion efficiency and mechanical strength compared to pure paraffin. The regression rate of these blended fuels was found to be less augmented compared to pure paraffin. Our previous study found that adding metallic additives can enhance the low

regression rate performance of paraffin-PE blended fuel [19]. The inclusion of nano and micro aluminum additives can improve the structural performance of paraffin-based fuel [20].

Boron is considered a prospective metallic fuel additive for rocket applications, including solid propellants and high-pressure explosives. It is best suited for volume-restricted propulsion systems due to its high gravimetric and volumetric heats of combustion [10,21]. Nonetheless, boron particles can be ignited without complete combustion due to thin oxide layers ( $B_2O_3$ ), thus preventing its widespread application in solid fuel. Various techniques are being studied to eliminate these problems, such as using fluoride-based dopants or dual metallic additives (magnesium-boron composite) to lower the boron particle ignition temperature [22]. The major benefit of magnesium diboride ( $MgB_2$ ) is that it is much more stable and easy to handle than metal hydrides. Moreover, the utilization of  $MgB_2$  can avoid a closed oxide layer formed during the combustion process.  $MgB_2$  has superconductor properties and high experimental heat of combustion (experimental: 23,943 J/g, theoretical 38,781 J/g) compared to elemental boron (22,465 J/g, theoretical 23,943 J/g) [21,22]. In addition,  $MgB_2$  exhibits a higher density ( $2.55 \text{ g/cm}^3$ ) than that of boron ( $2.37 \text{ g/cm}^3$ ) [22]. Using  $MgB_2$  as an additive in paraffin wax can improve fuel density, ultimately enhancing the hybrid launch vehicle performance. Bertoldi et al. [23] investigated the effects of  $MgB_2$  on mechanical and combustion characteristics of paraffin-based fuel. It was found that the inclusion of the  $MgB_2$  additive-enhanced the regression rate and mechanical performance. However, their regression rate tests at higher  $MgB_2$  loading were unsuccessful and did not fully understand combustion behavior.

Thus, in this study, the  $MgB_2$  and carbon black were added to paraffin wax to understand the thermal, mechanical, and ballistic performance. Thermogravimetry analysis (TGA) was used to analyse the melting, thermal stability, and decomposition behavior of these paraffin-based fuels. The uniaxial tensile and hardness tests were performed to evaluate the mechanical performance. Finally, lab-scale ballistic tests were carried out to study the combustion and regression characteristics under a gaseous oxygen environment. Further, the experimental and ideal characteristic velocities and characteristic velocity efficiency of paraffin-based fuels were evaluated. The combustion analysis of condensed combustion products was performed to predict the combustion behavior of  $MgB_2$  under an oxygen environment. The high temperature (473 K–1723 K) oxidation process of  $MgB_2$  was described using Thermogravimetry analysis, and a combustion model of these reactions was discussed.

## 2. Materials and methods

### 2.1. Materials

In this study, the pure paraffin wax (CAS No. 8002-74-2), analytical grade purity, was used as a fuel matrix and procured from Sigma-Aldrich (USA). The magnesium diboride (Purity

of  $\geq 99.5\%$ ; CAS No. 12007-25-9) was used to increase the energy density of the fuel, whereas carbon black (CAS No. 215-609-9) was added to enhance the radiation absorption of the fuel matrix. Both energy additives were supplied from Sigma-Aldrich (USA). The properties of the fuel matrix and additives are listed in Table 1.

### 2.2. Fuel preparation

Three formulations of paraffin-based fuel were prepared for thermal, mechanical, and ballistic characterization. The pure paraffin fuel samples were manufactured as reference fuel for comparison (Table 2). The fuel samples for ballistic performance were casted in a circular-port shape using a typical melt method [19]. The required amount of paraffin wax was heated in a bowl over the electric heater at a temperature of 393 K. The requisite quantity of additives (CB/ $MgB_2$ ), stored under the  $N_2$  environment, was accurately weighed and added to molten paraffin wax. The mixture was continuously stirred for 15–20 min to attain homogeneity. Finally, the mixture was poured slowly and continuously into a casting mold of length 200 mm and a port diameter of 15 mm. Before casting the fuel, a fine coating of oil was applied inside the edges of the casting mold to avoid the adhesiveness of paraffin with mold. Such coating facilitates the easier removal of fuel grain after solidification of paraffin. Our previous study found that paraffin wax tends to volumetric shrinkage (15%–25%), depending on the grade of wax, upon solidification from liquid to a solid phase [24]. Therefore, during the fuel casting, the molten paraffin mixture was poured slowly and in a single stretch into casting mold to avoid air bubbles formations and any other discontinuities in the fuel grain. The prepared fuel grain was stored at room temperature for

**Table 1** Properties of fuel matrix and additives.

Properties	Paraffin	Carbon black	Magnesium diboride
Chemical formula	$C_{28}H_{58}$	C	$MgB_2$
Density ( $\text{g/cm}^3$ )	818	0.21	2.57
Melting point (K)	335	3823	1073
Particles size	Solid crystal	20–40 $\mu\text{m}$	10 nm
Molecular weight	590	12.011	45.93

**Table 2** Tested paraffin-based fuel formulations.

Sample	Paraffin wax (wt%)	$MgB_2$ (wt%)	Carbon black (wt%)
P100	100	—	—
P-CB2	98	—	2
P- $MgB_2$	90	10	—
P-CB- $MgB_2$	88	10	2

curing and trimmed to the desired dimension, as shown in Figure 1. Visual inspection of the fractured surface of the fuel grain was carried out and observed to be free from any significant cracks or bubbles along the grain length.

### 2.3. Mechanical characterization

For mechanical performance, the ultimate tensile strength, elastic modulus, and hardness of paraffin-based fuel were evaluated using an INSTRON (3382)-25-kN universal testing machine and penetrometer, respectively. The tensile test specimens were prepared in dumb-bell shape according to the ASTM D638 standard [25]. The dimensions of the specimen were 7 mm thick, 29 mm wide, and a gauge length of 57 mm. All the tests were performed at a 50 mm/min crosshead speed in standard ambient conditions (298 K and 1 bar). The prepared standard tensile specimens are shown in Figure 2. The hardness tests were carried out using the ASTM D1321 standard [26] at 298 K. The specimen was kept under-sample holder, and the penetrator needle was aligned to the fuel surface without moving it down. The measurement accuracy was 0.1 mm of penetration depth.

### 2.4. Thermal characterization

The thermal characterization of paraffin-based fuel was performed on a thermogravimetric analyser (TGA-1500) instrument. The 3–5 mg of fuel sample was used to examine the thermal stability and decomposition behavior. The low-

temperature thermal decomposition study was performed at a 10 K/min heating rate under an  $N_2$  atmosphere. The sample scanned up to a temperature of 1073 K at a 50 ml/min mass flow rate of  $N_2$  gas. Differential scanning calorimetry (DSC) experiments were carried out with PerkinElmer Differential Scanning Calorimeter (Pyris 6 DSC) under an air atmosphere. A suitable quantity of samples ( $\sim 3$  mg) was placed in aluminum pans and heated from room temperature to 423 K at a 10 K/min scanning rate.

The high-temperature oxidation process of  $MgB_2$  was studied at a 10 K/min heating rate under an air atmosphere. Further, furnace tests have been performed to investigate the various oxides and oxidation products formed during the combustion of  $MgB_2$ . The  $MgB_2$  samples were heated at 1133 K, 1343 K, and 1603 K, respectively, in the airflow, using the Nabertherm burnout furnace.

### 2.5. Ballistic characterization

A series of ballistic tests were conducted on a lab-scale static motor under gaseous oxygen as an oxidiser. The test setup integrates various components: a lab-scale rocket motor, thrust stand, oxidiser feed system, pyrogen igniter and data acquisition system. Figure 3(a) depicts a schematic of a lab-scale static hybrid motor. The hybrid motor consists of an oxidiser settling chamber of length 33 mm and a diameter of 55 mm. An axial flow injector made of stainless steel plate with a 47 mm pitch circle diameter was used to supply the oxidiser into the combustion chamber.



Figure 1 Casted  $MgB_2$ -paraffin fuel grain.

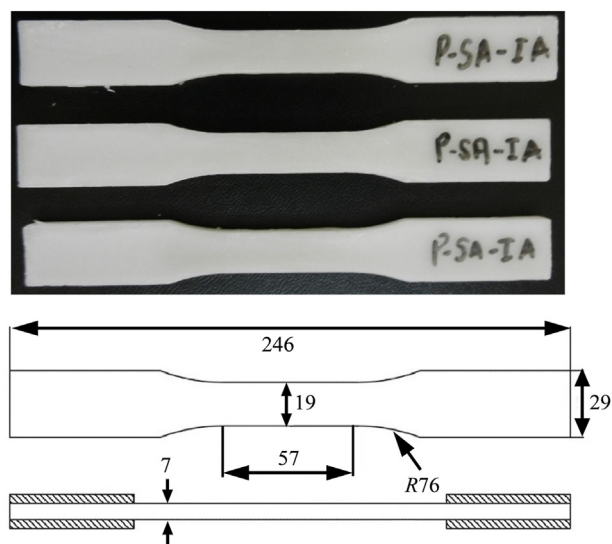
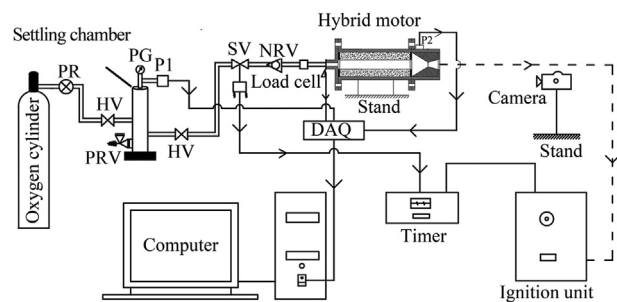
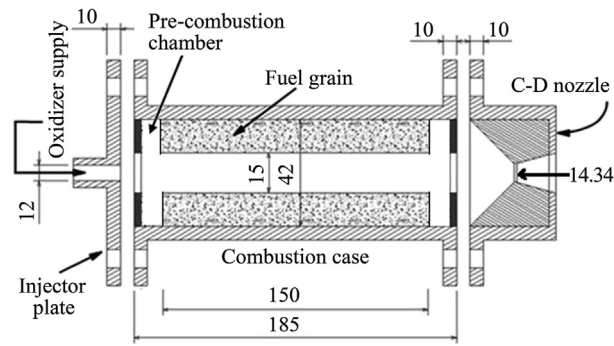


Figure 2 The fabricated tensile test specimen.



(a)



(b)

Figure 3 (a) Schematic of hybrid rocket test facility, (b) schematic of ballistic evaluation hybrid motor (all dimensions in mm).

A combustion chamber with 185 mm length and 42 mm inner diameter was provided to accommodate the fuel grain (Figure 3(b)). A 20 mm long post-combustion chamber was granted for better combustion of the un-burnt paraffin droplets in the combustion chamber before it exits the nozzle. A pre-combustion chamber of 15 mm length from the head end of the motor was allowed to ensure better mixing of oxidiser and fuel vapor. The role of the pre-chamber is to pre-heat the main chamber. The igniter at the head end of the motor will generate an initial heat source in the chamber to exceed the ignition temperature of the fuel grain. This process pre-heats the chamber, allowing the fuel to evaporate and react effectively when the oxygen is introduced. A convergent-divergent nozzle with a throat diameter of 14.34 mm made of steel, 45° semi-convergent, and 13° semi-divergent angle was used. A pyrotechnic solid propellant igniter was preferred because of its manufacturing simplicity and ease of installation. A small amount of solid propellant (~ 1 g) was ignited using a Nichrome wire wrapped around it to initiate solid fuel combustion. The firing tests were performed at a nozzle expansion ratio ( $A_e/A_t$ ) of 2.09.

A pressure regulator and a solenoid valve regulated and controlled the oxidiser mass flow rate. All the fuel formulations were tested under the oxidiser mass flux range of 75.7 kg/(m<sup>2</sup>·s) to 130.4 kg/(m<sup>2</sup>·s). After a predetermined burn time (2.38 s–2.85 s), the combustion was terminated by shutting down the oxidiser supply with the help of a solenoid valve and PT 380 sequential timer. The static lab-scale hybrid motor (Figure 4(a)) and firing test of pure paraffin and MgB<sub>2</sub> fuels are shown in Figure 4(b)(c). The regression rate and fuel mass consumption were the post-test measurements.

### 2.5.1. Data reduction

The regression rate was estimated using the mass loss technique, which is the most accurate and widely used method [27]. The average regression rate of paraffin-based fuel was calculated by Eq. (1).

$$\dot{r} = \frac{d_b - d_{ig}}{2t_b} \quad (1)$$

where  $d_b$  and  $d_{ig}$  are the diameter of the fuel port after combustion and before its ignition, respectively. The  $t_b$  is the burn time between the start of the ignition process and the termination of the oxidiser supply. The post-combustion fuel port diameter was calculated using the following Eq. (2).

$$d_b = \sqrt{\left( d_{ig}^2 + \frac{\dot{m}_b}{\pi \rho_f l_f} \right)} \quad (2)$$

where  $\rho_f$  is the density of solid fuel,  $m_b$  denotes the burnt mass of fuel and  $l_f$  indicates the fuel length. During the combustion process, the paraffin fuel droplets generated from the melted liquid layer are not completely burned



(a)



(b)



(c)

**Figure 4** (a) A lab-scale hybrid test motor on firing stand, (b) static firing test of pure paraffin, (c) static firing test of P-CB-MgB<sub>2</sub>.

throughout the fuel grain port and through the exhaust nozzle. Therefore, the uncertainty of the final unburned fuel mass was roughly approximated at 5% of the final mass due to the spallation of unburned mass from the motor. The average oxidiser mass flux was evaluated by Eq. (3)

$$G_{ox} = \frac{\dot{m}_{ox}}{A_p} \quad (3)$$

where  $A_p$  is the fuel port cross-sectional area and  $\dot{m}_{ox}$  is the mass flow rate of the oxidiser. It was calculated by taking the average post-combustion fuel port diameter and before the ignition process (Eq. (4))

$$A_p = \frac{\pi}{4} \left( \frac{d_b + d_{ig}}{2} \right)^2 \quad (4)$$

### 3. Results and discussion

#### 3.1. Mechanical performance

The mechanical performance of fabricated paraffin-based fuels was examined under tensile, impact, and hardness modes. In fact, one of the major issues with paraffin-based fuels is the poor mechanical properties; therefore, an improvement by means of additives is highly required. All prepared fuel samples were tested three times, and Table 3 shows the average test parameters value from statistical analysis. The statistical average values of elastic modulus and ultimate tensile strength indicate the uniformity of a prepared sample as well as the reproducibility of tests. The stress-strain curves of the paraffin-based fuels are presented in Figure 5. All the formulations studied exhibited similar stress-strain behavior, close to that of pure paraffin samples. All tested samples displayed brittle behavior along the stress-strain curves, and fillers into paraffin increased the mechanical performance. Adding 2 wt% CB to the paraffin slightly enhanced the ultimate tensile strength and elastic modulus compared to the pure paraffin sample. This study used a micro-size CB filler with an average diameter of 25  $\mu\text{m}$ . In Figure 6(a), the paraffin lumps can be observed, and the connections between these lumps are not dense. The lower mechanical strength of the P-CB2 sample is due to the weak interfacial adhesion between the CB filler and paraffin matrix [28]. The applied tensile load could have partially transferred to the paraffin matrix through CB filler which could be responsible for low improvement. Ryu et al. [29] explained that the addition of nanofiller improved the mechanical performance of paraffin-based fuel compared to that of sample loaded with the micro size filler.

With nano  $\text{MgB}_2$  formulation, the tensile properties were significantly improved compared to the pristine paraffin sample. The ultimate tensile strength was increased to 40%, whereas the stiffness improved by 36% (Table 3). When CB was added to the P- $\text{MgB}_2$  formulation, an increment in the ultimate tensile strength of 21% was observed, whereas the elastic modulus was decreased by 3% compared to pure paraffin. The influence of CB additive on the ductility was not positive. Adding 2 wt% of CB in P- $\text{MgB}_2$  sample declines the critical strain from maximum value to 17%. Whereas the addition of  $\text{MgB}_2$

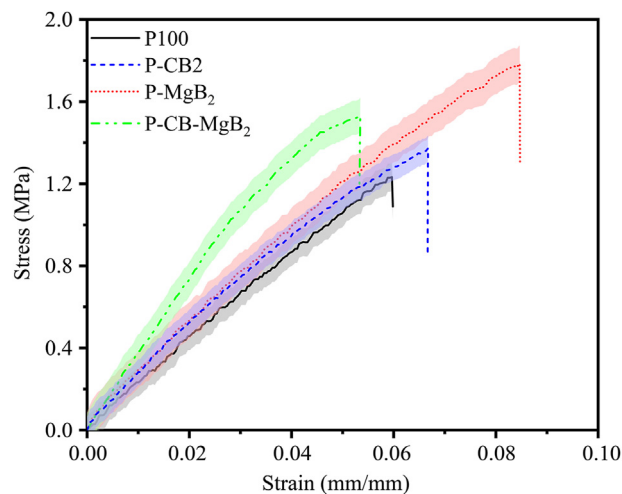


**Figure 5** A typical average stress-strain curves of the paraffin-based fuels.

shown an improvement in the critical strain at the break, which is 33% higher than that of pure paraffin formulation. A similar trend was also observed with energy at the break, which quantifies the toughness of the tested specimen. Doping the  $\text{MgB}_2$  (at 10 wt% loading) into paraffin wax showed a maximum value of 0.68 J, a 48% improvement over that of pure paraffin wax (Table 3). The lowest toughness of 0.46 J was observed with a pure paraffin wax sample.

In the case of  $\text{MgB}_2$  filler, the increased mechanical properties must be caused by strong interfacial interaction between nanofiller and paraffin matrix (Figure 6(b)). The nano  $\text{MgB}_2$  filler provides a very large surface area in contact with the paraffin matrix, which acts as a reinforcement to transfer the applied load [30]. On the other hand, mechanical performance slightly decreased when CB filler was added to P- $\text{MgB}_2$ , which is ascribed probably to micro-sized CB fillers acting as mechanical failure concentrators [31–33]. However, the P-CB- $\text{MgB}_2$  sample still has higher ultimate tensile strength compared to pure paraffin. Several other researchers reported similar results [34–36], which suggest that the addition of nanofiller particles improves the interaction between the filler and the matrix. Therefore, nanofiller in paraffin-based fuel can significantly improve mechanical interfacial resistance and transfer the applied load from the fuel matrix to the filler.

**Table 3** Mechanical test parameters of paraffin-based fuels.

Sample	Ultimate tensile strength (MPa)	Elastic modulus (MPa)	Critical strain	Energy at break (J)	Needle penetration, @298 K (0.1d-mm)
P100	1.30 $\pm$ 0.09	64.05 $\pm$ 6.7	0.06 $\pm$ 0.004	0.46 $\pm$ 0.04	22.33 $\pm$ 0.2
P-CB2	1.38 $\pm$ 0.07	65.37 $\pm$ 5.8	0.06 $\pm$ 0.004	0.56 $\pm$ 0.03	19.20 $\pm$ 0.2
P- $\text{MgB}_2$	1.82 $\pm$ 0.06	86.80 $\pm$ 2.1	0.08 $\pm$ 0.002	0.68 $\pm$ 0.03	18.33 $\pm$ 0.3
P-CB- $\text{MgB}_2$	1.57 $\pm$ 0.04	61.94 $\pm$ 4.2	0.05 $\pm$ 0.003	0.49 $\pm$ 0.05	15.17 $\pm$ 0.5

( $\pm$ SD)-Standard deviations.

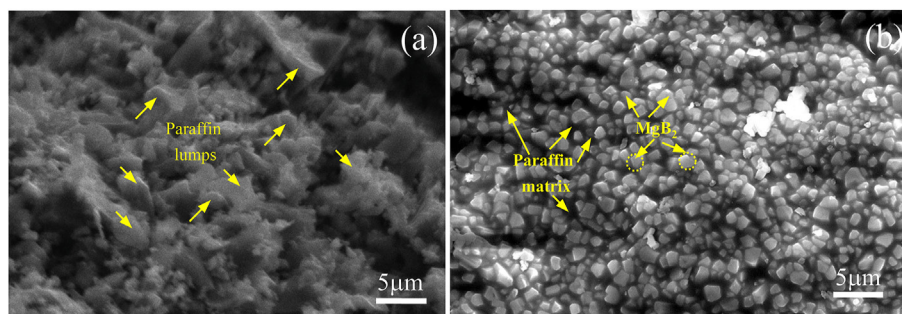


**Figure 6** SEM images of fracture (a) P-CB2 tensile sample, (b) P-MgB<sub>2</sub>.

The penetration test is one of the most popular techniques for calculating the hardness of paraffin-based fuel. From Table 3, it can be observed that the average penetration depth of the pure paraffin sample is 22.33 mm. The addition of CB filler into the paraffin increased the hardness of the sample, which is revealed by the lower penetration depth (19.20 mm). Compared to pure paraffin, the paraffin wax with 2 wt% MgB<sub>2</sub> loading exhibited high hardness (18.33 mm penetration depth). Its value was further reduced with the P-CB-MgB<sub>2</sub> composite sample, where the penetration depth was found to be 15.17 mm. Therefore, adding inorganic fillers shows a strong interaction in the wax matrix and improves the hardness of paraffin-based fuel. This can be attributed to the filler material, which acted as reinforcement to carry the loads and stresses [16,37]. The fillers can also reduce the movement of the discontinuities, voids, or air bubbles created during the fabrication of the fuel sample. The average penetration depth of the P-CB-MgB<sub>2</sub> sample was the lowest among all tested formulations. It is ascribed to the synergy effect of CB and MgB<sub>2</sub> fillers. The paraffin matrix received the penetration energy shared by the MgB<sub>2</sub> filler, whereas the CB acted as a compatible filler to control the shrinkage of wax during solidification [28]. The structural performance results of paraffin-based fuel presented here are insufficient to accurately predict the actual loads encountered during the flight. Since the full-scale motor grain would be subjected to various stress loads, axial thrust load, and radial combustion pressure during the operation. Therefore, a full assessment of mechanical performance under such loading conditions and environment needs to be carried out in the near future.

### 3.2. Thermal characterization

Figure 7(a) shows the thermogravimetric analysis curves for pure paraffin and the sample loaded with CB and MgB<sub>2</sub>. It can be observed that major mass loss of pure paraffin sample occurred in a single step. The onset decomposition temperature of paraffin was observed at around 522 K, which corresponds to the decomposition of low molar mass chains [38]. The addition of CB additives into paraffin increased the thermal stability, and the initial decomposition of the P-CB2 sample started at around 544 K. In fact, the black carbon addition enhanced the thermal stability by

decreasing the chain mobility. This decrease in chain mobility also affects the melting temperature [39].

However, the decomposition of the paraffin sample loaded with CB filler was observed in two steps. The second decomposition step occurred in the temperature range of 773 K–973 K, which ascribed to the decomposition and evaporation of the high-temperature resistance fillers (carbon black) and the higher molar carbon chain [19].

With the P-CB-MgB<sub>2</sub> sample, the initiation of decomposition started around 540 K, as shown in Table 4. The presence of CB and MgB<sub>2</sub> additives promoted the decomposition, and definite mass loss in the second stage was observed in the range of 723 K–973 K. On the other hand, the addition of CB into paraffin shifted the decomposition stages to a slightly higher temperature (Table 4). The effect of these additives on thermal decomposition can be correlated to enhanced thermal conductivity and heat capacity of paraffin-based fuel [28]. The presence of additives in the paraffin matrix absorbed more heat and resulted in the degradation of the polymer chain at higher temperatures [40].

In fact, hybrid rocket engines are well known for their stop and restart-ability over solid rockets. Therefore, fuel grain will be subjected to more than one ignition, burnout, and re-ignition phases during the rocket operation. It is important to know the performance of the grain when it is re-ignited. The re-ignition ability of paraffin-based fuel can be characterised by understanding the melting behavior under reheating conditions. Since the stability of the liquid melt layer formed over the fuel surface is directly related to the melting temperature of the fuel [41]. The low melting temperature of fuel can degrade a large amount of fuel into the combustion zone. Therefore, differential scanning calorimetry (DSC) experiments with reheating conditions were performed to understand the melting behavior of paraffin-based fuels. When reheating was performed, it was observed that all fuel formulations exhibited a reduction in melting temperature (Figure 7(b)). Also, the melting enthalpies of samples were reduced in reheating compared to that of the first heating condition. In short, paraffin samples loaded with CB showed the highest melting temperature and melting enthalpy reduction among all the tested fuel formulations. Fernandes et al. [38] predicted that adding additives tends to increase the melting temperature of paraffin,

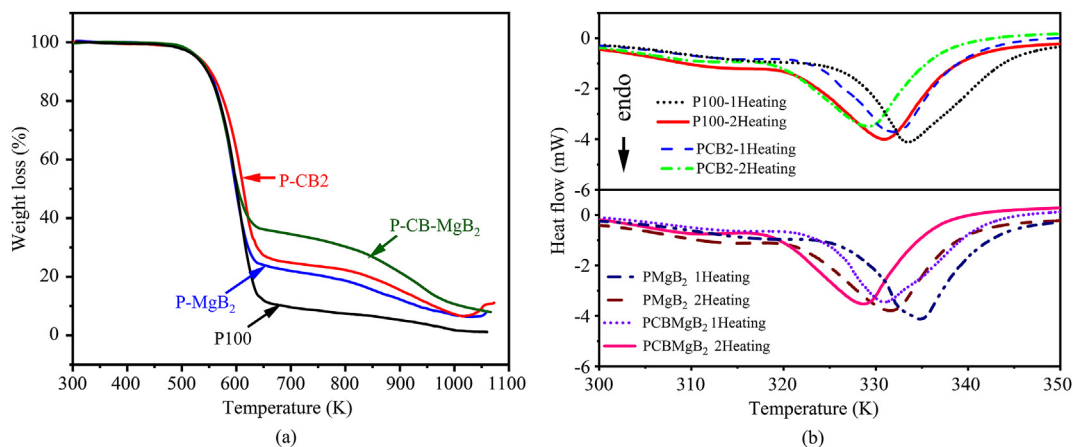


**Figure 7** Low-temperature thermal analysis of paraffin-based fuel (a) TGA curves, (b) DSC curves.

**Table 4** TGA and DSC measurement parameters of paraffin-based fuel.

Sample	Onset decomposition temperature (K)	Maximum decomposition temperature (K)	Melting point (K)		Melting enthalpy (J/g)	
			1st heating	2nd heating	1st heating	2nd heating
P100	522	606.6	333.93	330.87	174.3	165.2
P-CB2	544	622.3	331.76	329.13	171.4	133.6
P-MgB <sub>2</sub>	536	609.4	334.61	331.38	176.8	170.3
P-CB-MgB <sub>2</sub>	540	615.6	331.96	328.58	169.3	126.1

whereas; the inclusion of CB can oppose this effect. In addition to melting temperature and melting enthalpy, the irregular shape of the additive particles indicates a higher surface reactivity (per unit surface area) in the oxygen chemisorption process, which is the first stage before ignition [42]. Mandilas et al. [42] discussed several factors such as average primary particle morphology and nanopowder composition that could alter the established trend of increasing particle reactivity with decreasing average primary particle size. The particle with an irregular shape has a higher surface area and is consequently more reactive than the particle with a spherical shape. The irregular shape of particles arguably implies a greater surface reactivity in the oxygen chemisorption process, which is the first step prior to ignition. However, the actual operating conditions in hybrid rocket combustion are quite different from the current heating rates of TG/DSC simulation. Based on these results, the low-temperature decomposition, melting, and enthalpy associated with these additives-loaded paraffin-based fuels can be used as valuable inputs for modeling combustion and energetic formulations.

### 3.3. Regression rate studies

Lab-scale ballistic tests were carried out to evaluate the regression rates performance of paraffin-based fuels loaded with CB and MgB<sub>2</sub> additives. The average linear regression rate of paraffin-based fuels measured over a mass flux range of 75.7 kg/(m<sup>2</sup>·s) to 130.4 kg/(m<sup>2</sup>·s) is shown in Figure 8

and Table 5. The average linear regression rates were evaluated using the mass-loss technique since the measurement uncertainty associated with this technique is minimum compared to other methods [27]. The uncertainty in the measurement was evaluated based on the root-sum-square uncertainty rule [43]. The uncertainties in measurement are presented in Table 6.

The regression rates of pure paraffin and HTPB [44] fuels at an oxidiser mass flux range of 76.2 kg/(m<sup>2</sup>·s) to 127.8 kg/

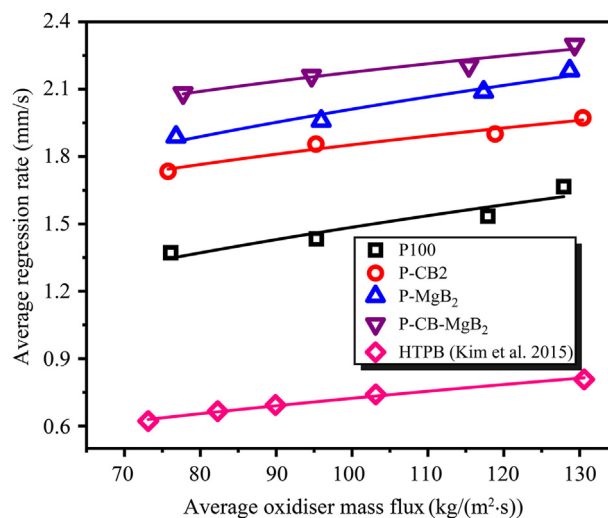


**Figure 8** Average regression rates vs oxidiser mass flux variation for paraffin-based fuels.

**Table 5** Regression rate data from ballistic test evaluation motor.

Fuel sample	Fuel density (kg/m <sup>3</sup> )	Burn time (s)	Final diameter (mm)	Oxidiser mass flux $G_{ox}$ , (kg/(m <sup>2</sup> ·s))	Regression rate (mm/s)	Regression rate parameters	
						$a$	$n$
P-CB-MgB <sub>2</sub>	821	2.85	26.86	77.7	2.082	0.61 ± 0.03	0.24 ± 0.01
	821	2.38	25.28	94.7	2.16		
	821	2.78	27.25	115.4	2.204		
P-MgB <sub>2</sub>	821	2.54	26.67	129.3	2.298	0.68 ± 0.028	0.22 ± 0.01
	826	2.71	25.23	76.8	1.888		
	826	2.56	25.02	95.9	1.958		
	826	2.45	25.23	117.3	2.088		
P-CB2	826	2.75	27.1	128.7	2.183	0.55 ± 0.021	0.28 ± 0.02
	823	2.78	24.64	75.7	1.734		
	823	2.82	25.46	95.2	1.855		
	823	2.7	25.26	118.9	1.9		
P-100	823	2.55	25.05	130.4	1.972	0.61 ± 0.0311	0.2 ± 0.01
	818	2.51	23.61	76.1	1.371		
	818	2.85	25.31	95.3	1.433		
	818	2.44	24.26	117.9	1.534		
	818	2.76	25.71	127.9	1.666		

Initial port diameter = 15 mm, fuel grain length = 150 mm.

(m<sup>2</sup>·s) were also presented in Figure 8 for comparison. It can be observed that the addition of 2 wt% of CB into paraffin has reasonably improved the regression rate. At low oxidiser mass flux (75.7 kg/(m<sup>2</sup>·s)), the regression rate increased by 26% compared to pure paraffin, whereas 30% and 18% improvement was seen with intermediate and highest oxidiser mass flux, respectively. The CB in the condensed phase acts as an opacifier, absorbs a portion of the heat produced by combustion in the flame zone, and rapidly transfers it to the solid fuel. It is widely used in solid fuel fabrication to increase the absorptivity of grain [45]. Therefore, the regression rate enhancement can be ascribed to radiation heat transfer from the CB particles at the combustion zone to the surface of the fuel. Carmicino et al. [45] shown that the addition of 3 wt% CB into HTPB fuel enhanced the regression rate up to 30%.

Under the same operating condition, the regression rate of the tested paraffin fuel loaded with MgB<sub>2</sub> shows a similar

enhancement trend. The regression rate was improved from 38% at the low oxidiser mass flux (76.8 kg/(m<sup>2</sup>·s)), to 36% at the intermediate flux range (95.9 kg/(m<sup>2</sup>·s)) to 30% calculated at the highest oxidiser flux (128.7 kg/(m<sup>2</sup>·s)) when compared to pure paraffin. In the P-CB-MgB<sub>2</sub> fuel sample, the regression rate was increased to 52% at low oxidiser mass flux (129.3 kg/(m<sup>2</sup>·s)), while at the intermediate flux range (94.7 kg/(m<sup>2</sup>·s)), the regression rate improved by 51%. At the high oxidiser mass flux (77.7 kg/(m<sup>2</sup>·s)); the improvement in regression rate was reduced to 38% compared to pure paraffin. MgB<sub>2</sub> has a high heating value, superconducting properties, and stability at room temperature [46,47]. During the combustion, the MgB<sub>2</sub> could be ejected off the fuel surface and reach the flame zone. In the high-temperature flame zone, a large amount of heat was released due to the combustion of the Mg oxide layer and transferred to the solid fuel surface, which ultimately generated a large amount of fuel mass. De Morais

**Table 6** Measurement uncertainty analysis based on the root-sum-square uncertainty rule.

Parameters	Uncertainty analysis	Uncertainty equation
<sup>a</sup> Regression rate ( $\dot{r}$ )	±0.23 mm/s	$\zeta_{\dot{r}} = \sqrt{\left[\left(\frac{\partial \dot{r}}{\partial d_b} \zeta_{d_b}\right)^2 + \left(\frac{\partial \dot{r}}{\partial d_{ig}} \zeta_{d_{ig}}\right)^2 + \left(\frac{\partial \dot{r}}{\partial t_b} \zeta_{t_b}\right)^2\right]}$
<sup>b</sup> Oxidiser mass flux ( $G_{ox}$ )	±3.2	$\zeta_{G_{ox}} = \sqrt{\left[\left(\frac{\partial \dot{r}}{\partial \dot{m}_{ox}} \zeta_{\dot{m}_{ox}}\right)^2 + \left(\frac{\partial \dot{r}}{\partial A_p} \zeta_{A_p}\right)^2\right]}$
<sup>c</sup> C*	±6.4%	$\zeta_{C^*} = \sqrt{\left[\left(\frac{\partial \dot{r}}{\partial A^*} \zeta_{A^*}\right)^2 + \left(\frac{\partial \dot{r}}{\partial P_c} \zeta_{P_c}\right)^2 + \left(\frac{\partial \dot{r}}{\partial \dot{m}} \zeta_{\dot{m}}\right)^2 + \left(\frac{\partial \dot{r}}{\partial \dot{m}_f} \zeta_{\dot{m}_f}\right)^2 + \left(\frac{\partial \dot{r}}{\partial t_b} \zeta_{t_b}\right)^2\right]}$

<sup>a</sup>Where,  $\zeta_{\dot{r}}$ ,  $\zeta_{d_b}$ ,  $\zeta_{d_{ig}}$ , and  $\zeta_{t_b}$  are the uncertainty in the regression rate, burn port diameter, initial port diameter and burn time, respectively.

<sup>b</sup>Where,  $\zeta_{G_{ox}}$ ,  $\zeta_{\dot{m}_{ox}}$ , and  $\zeta_{A_p}$  are the uncertainty in the oxidiser mass flux, oxidiser mass flow and port area, respectively.

<sup>c</sup>Where,  $\zeta_{C^*}$ ,  $\zeta_{A^*}$ ,  $\zeta_{P_c}$ ,  $\zeta_{\dot{m}_f}$ , and  $\zeta_{t_b}$  are the uncertainty in the characteristic efficiency, throat area, chamber pressure, fuel mass flow rate and burn time, respectively.

Bertoldi et al. [23] tested  $\text{MgB}_2$  loaded paraffin-based fuel and found that the inclusion of  $\text{MgB}_2$  additive improved the regression rate performance of hybrid rocket fuel. In our case, for the P-CB- $\text{MgB}_2$  fuel sample, the regression rate improvement can be ascribed to the synergetic effect of both CB and  $\text{MgB}_2$  additives.

The power-law approximation  $r = aG_{ox}^n$  as used to express the regression rate versus oxidiser mass flux trend. Where the oxidiser mass flux exponent ' $n$ ' and coefficient ' $a$ ' were calculated experimentally. The power-law approximations of all paraffin-based fuel formulations are shown in Table 5. It can be observed that the pure paraffin displayed low dependency ( $n = 0.2$ ) of the regression rate on the oxidiser mass flux.

The addition of the additives into paraffin resulted in relatively higher exponent values ( $n = 0.22$ – $0.28$ ), implying that the paraffin-based fuel exhibits a similar regression rate behavior as the oxidiser mass flux increases. In classical diffusion-limited theories, the value of oxidiser mass flux is reported as 0.8 [48], which is significantly higher than the value observed in paraffin-based formulation ( $n = 0.2$ – $0.28$ ). Paraffin-based fuel has shown a significant regression rate enhancement compared to pure paraffin and HTPB over the investigated oxidiser mass flux range. P-CB- $\text{MgB}_2$  exhibited the highest regression rate among the investigated paraffin-based fuel. The combustion efficiency of prepared paraffin-based fuel was evaluated based on experimental and ideal characteristic velocity. Characteristic velocity can be used as a tool to express the amount of energy produced during the combustion of these paraffin fuels [16]. Since characteristic velocity is a function of the fuel and oxidiser combination used and the efficiency of the combustion. In this study, the ideal characteristic velocity of fuel was estimated by NASA CEA code [49], whereas the experimental characteristic velocity was estimated by using the following Eq. (5)

$$C_{exp}^* = \frac{A^* \int_0^{t_b} P_c dt}{\int_0^{t_b} \dot{m} dt + \Delta m_f} \quad (5)$$

where  $A^*$  is the nozzle throat area and  $P_c$  is the average chamber pressure. Over the burn through time,  $t_b$ , the average mass flow rate of propellant ( $\dot{m}$ ), is calculated by the oxidiser and fuel mass flow rates. The degree of completeness of combustion was assessed through the efficiency of characteristic velocity using the following Eq. (6)

$$\eta_{C^*} = \frac{C_{exp}^*}{C_{theo}^*} \quad (6)$$

The experimental and theoretical characteristic velocities for each set of fuel combinations at varying O/F ratio is presented in Figure 9. It is possible to note that the measured

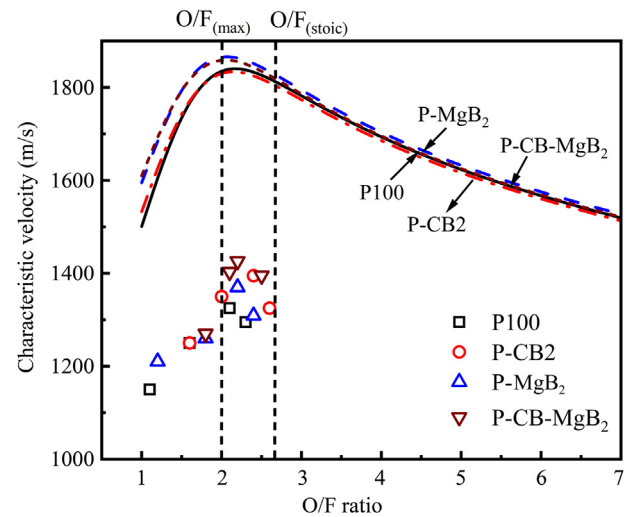


**Figure 9** Characteristic velocity variations as a function of oxidiser-to-fuel ratio for paraffin-based fuels.

characteristic velocity for each set of fuel stands in the range of 68%–79% of characteristic velocity efficiency. The stoichiometric  $(O/F)_{stoic}$  for the pure paraffin is 2.7 (Figure 10). The  $(O/F)$  that maximises the  $I_{sp}$   $(O/F)_{max}$  is found to be 2. This is also confirmed in the experimental work by Karakas et al. [50] that shows a decrease of the  $(O/F)_{max}$  when additives are added to pure paraffin.

In rocket applications, the specific impulse is one of the most important performance parameters to optimize. In this study, the experimental tests were performed with an oxidiser to fuel ratio of 1.5–2.6. Among each set of tested fuel formulations, a combination of  $\text{MgB}_2$  and CB with paraffin exhibited higher characteristic velocity efficiency and characteristic velocity, followed by paraffin with CB and paraffin with  $\text{MgB}_2$ . These results indicate that the  $\text{MgB}_2$ /CB additives ignited and burned more efficiently, resulting in large amounts of combustion products.

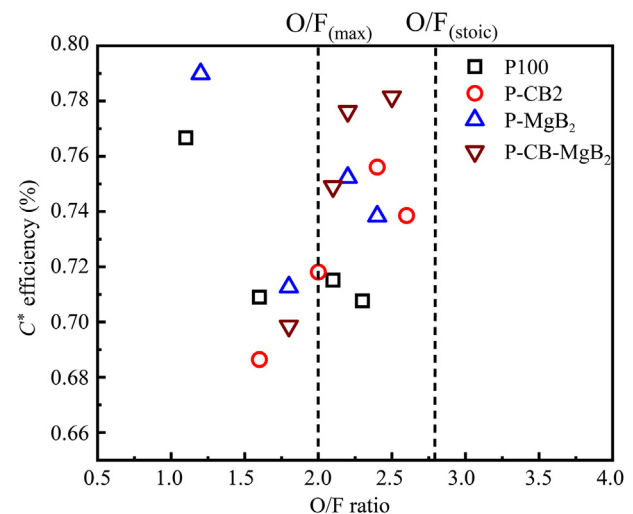


**Figure 10** Comparison of characteristic velocity efficiency vs oxidiser-to-fuel ratio for paraffin-based fuels.

Moreover, the incomplete combustion effect of pure paraffin fuel on characteristic velocity efficiency can be observed in the plume of the firing test (Figure 4(b)). During the combustion process, a large amount of fuel vapors were produced due to paraffin droplets entrainment, which was not fully burnt inside the combustion chamber. These paraffin droplets were ejected unburnt through the nozzle and burnt in the combustion plume outside the nozzle. Whereas, in the case of additives-loaded fuels, the carbon black acted as an opacifier and enhanced the radiation heat absorption of the paraffin [11,38]. Since the diffusion of radiation from the flame to the unmodified paraffin surface may have resulted in the uncontrolled shedding of fuel. Based on these findings, it can be hypothesised that the addition of additives such as  $MgB_2$  and CB into paraffin fuel can regulate the combustion efficiency and motor performance of the hybrid rocket.

### 3.4. Combustion mechanism of $MgB_2$

In order to understand the combustion behavior of  $MgB_2$ , the TG experiments were first performed in an air environment. Several events were observed on the TG curve of  $MgB_2$  (Figure 11). The entire  $MgB_2$  combustion mechanism comprises four distinct steps, which correspond to the temperature range of 473 K–1723 K. There was no significant weight gain until 889 K; however, as the temperature reached 673 K, approximately  $\sim 1\%$  weight loss was observed. Impurities are considered the source of such insignificant weight loss [47]. The oxidation of Mg increased with further temperature increases, resulting in weight gain. In step I, the  $MgB_2$  oxidation process peaks at 1076 K and occurs in the temperature range of 889 K–1135 K. Step I also composes the unoxidised  $MgB_2$  as a product. The weight gains of  $\sim 28\%$  were observed during step I, and an apparent exothermic peak can be seen in the DTG curve (Figure 11). Step II started at a temperature of 1135 K, and the sample gained a weight of 22.6% at

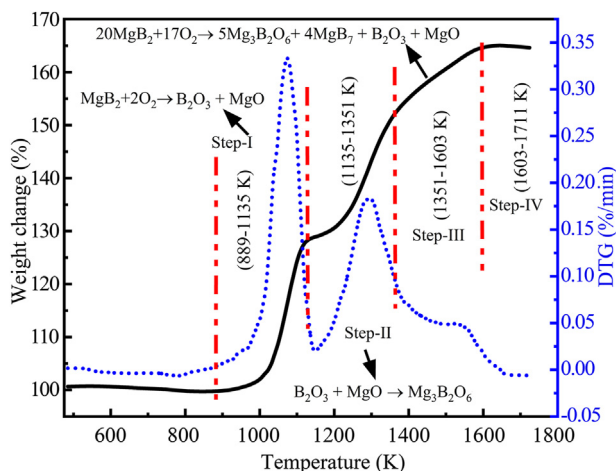


**Figure 11** TG/DTG curves represent the various steps of  $MgB_2$  oxidation.

the end of 1351 K. A strong exothermic peak at 1294 K was observed during the oxidation process. Step III extends from 1351 K to 1603 K, the energetic oxidation reactions occur with a weight gain of approximately 13.3%, and peak oxidation temperature corresponds to 1553 K. Step IV range from 1603 K to 1711 K and is associated with a weight gain of 1.3% of the original weight, which is significantly small compared to that of step I. This indicates that the evaporation of Mg and the oxidation process appear nearly complete.

It is difficult to further identify and analyse thermal oxidation products due to the small amount of samples used in the TG apparatus. Therefore, furnace tests were performed after the TG measurement to investigate the oxides and oxidation products formed on  $MgB_2$  during the various steps (I-IV). The  $MgB_2$  samples were heated in the flow of air using the Nabertherm burnout furnace. To examine the composition of the oxidation products formed in step I, the  $MgB_2$  sample was heated up to 1133 K. The oxidation products mainly comprise magnesium oxide (MgO) and unoxidised  $MgB_2$ . The hindering effect of reactant diffusion through the oxide layer is negligible, and the liner slope can be seen on the TG curve (step I), indicating that the oxidation reaction is proceeding smoothly. The following reaction (1) occurred during the first step of  $MgB_2$  oxidation:



The oxidation products of step I were examined using XRD and SEM analysis. In Figure 12, It can be seen that most of the XRD peaks are mainly composed of MgO (JCPDS card No. 79-0612) and  $MgB_2$  (JCPDS card No. 04-2014; JCPDS card No. 04-018-7387). To study the morphology of  $MgB_2$  before and after the oxidation process, the collected residues were further investigated by SEM. Figure 13(a) shows the SEM images of  $MgB_2$  before the

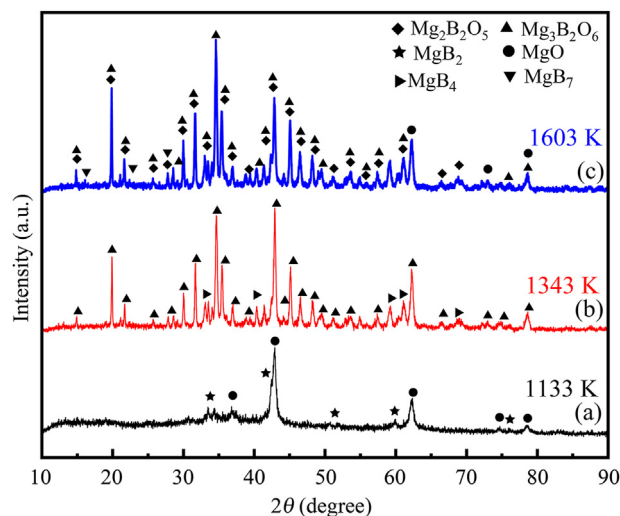


**Figure 12** XRD pattern of the post-combustion residue of  $MgB_2$  (a) 1133 K, (b) 1343 K and (c) 1603 K.

oxidation process, and Figure 13(b) represents the MgB<sub>2</sub> residue heated up to 1133 K. The MgB<sub>2</sub> sample reveals irregularly shaped hexagonal grains with good crystallinity before oxidation. Whereas the crystallinity slightly disappeared after the oxidation process, which can be attributed to the solid-liquid phase transformation of MgB<sub>2</sub>. It is interesting to note that intensely bright areas (Figure 13(b)) reveal the formation of the MgO phase in step I, which is also supported by XRD results.

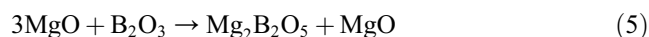
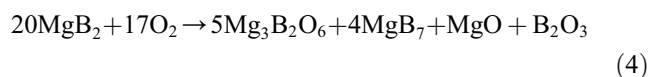
The composition of oxidation products formed in step II was examined by heating the fresh MgB<sub>2</sub> sample at 1343 K. The oxidation products of MgB<sub>2</sub> from step I, MgO, and B<sub>2</sub>O<sub>3</sub>, will further react to form Mg<sub>3</sub>B<sub>2</sub>O<sub>6</sub> phase in step II. The formation of Mg-B-O ternary oxide and Boron-rich phase MgB<sub>4</sub> can be expressed by the following reactions (2), (3):



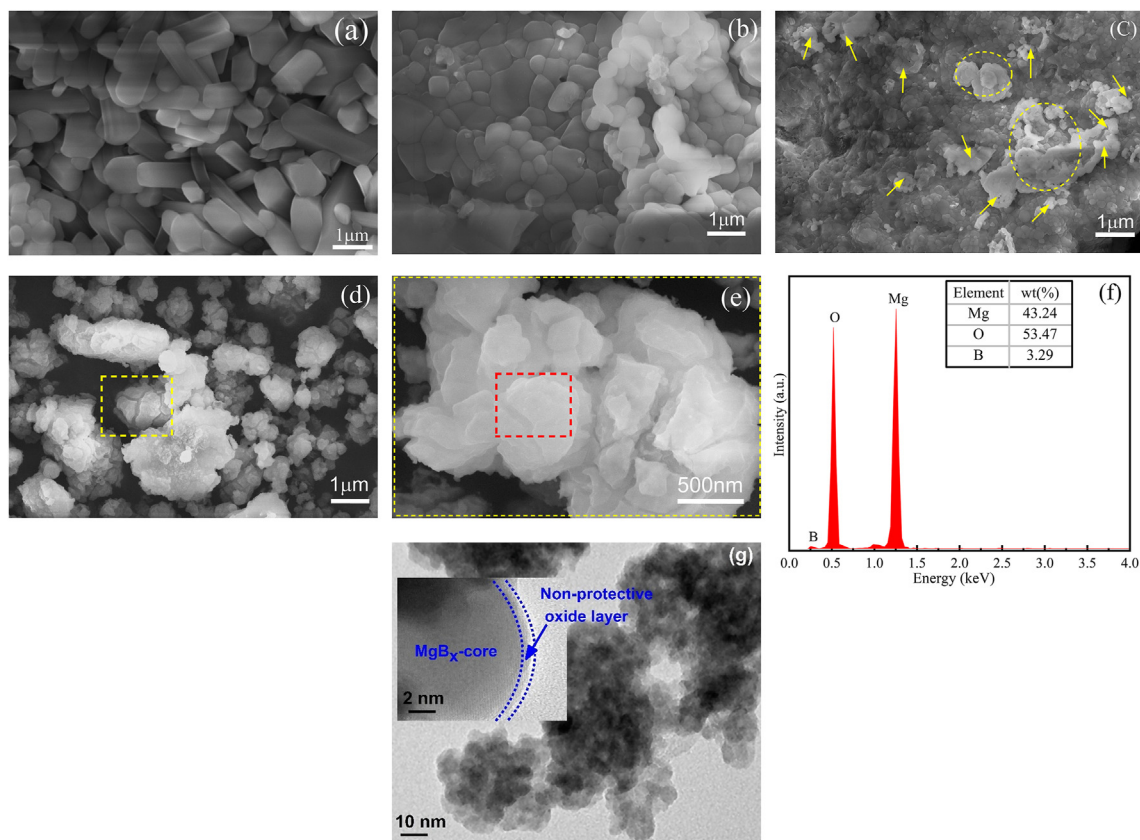
The MgB<sub>4</sub> (JCPDS card No. 73-1014) and Mg<sub>3</sub>B<sub>2</sub>O<sub>6</sub> (JCPDS card No. 83-0625) were identified in the XRD pattern (Figure 12(b)). In step II, as the temperature raised to 1343 K, a rapid oxidation process could have released the Mg vapor and resulted in the MgB<sub>4</sub> and Mg<sub>2</sub>B<sub>2</sub>O<sub>5</sub> phases. The surface morphology of the residue is presented in

Figure 13(c), and it exhibited fine smooth morphology with non-protective layers compared to that of the residues of step I. Guo et al. [46] conducted similar oxidation experiments with MgB<sub>2</sub> in a tube furnace under an air environment. It was reported that stage I (850 K–1223 K) and stage II (1223 K–1343 K) exhibited a rapid oxidation process with the formation of a non-protective oxide layer, as in agreement with this study. The formation of such non-protective oxide layers can favor the diffusion paths along grain boundaries and release a large amount of heat in the combustion zone.

The fresh MgB<sub>2</sub> sample was further heated up to 1603 K under air and subjected to XRD and SEM analysis to investigate the oxidation products formed in step III. Under this temperature range, the sample is still in the oxidation process, and the oxidation products of the MgB<sub>2</sub> sample contain MgB<sub>4</sub>, MgO, Mg<sub>2</sub>B<sub>2</sub>O<sub>5</sub> and Mg<sub>3</sub>B<sub>2</sub>O<sub>6</sub> ternary oxides. The following reactions (4), (5) occurred in step III are:



The XRD pattern (Figure 12(c)) shows the presence of MgB<sub>7</sub>, Mg<sub>2</sub>B<sub>2</sub>O<sub>5</sub> and Mg<sub>3</sub>B<sub>2</sub>O<sub>6</sub> phases. It can be presumed



**Figure 13** SEM images of post-combustion residues of MgB<sub>2</sub> (a) unburnt MgB<sub>2</sub>, (b) MgB<sub>2</sub> heated at 1133 K, (c) MgB<sub>2</sub> heated at 1343 K, (d) MgB<sub>2</sub> heated at 1603 K, (e) magnified view of the image (e), (f) EDS scan of image (e), and (g) TEM images of MgB<sub>x</sub> oxide layer.

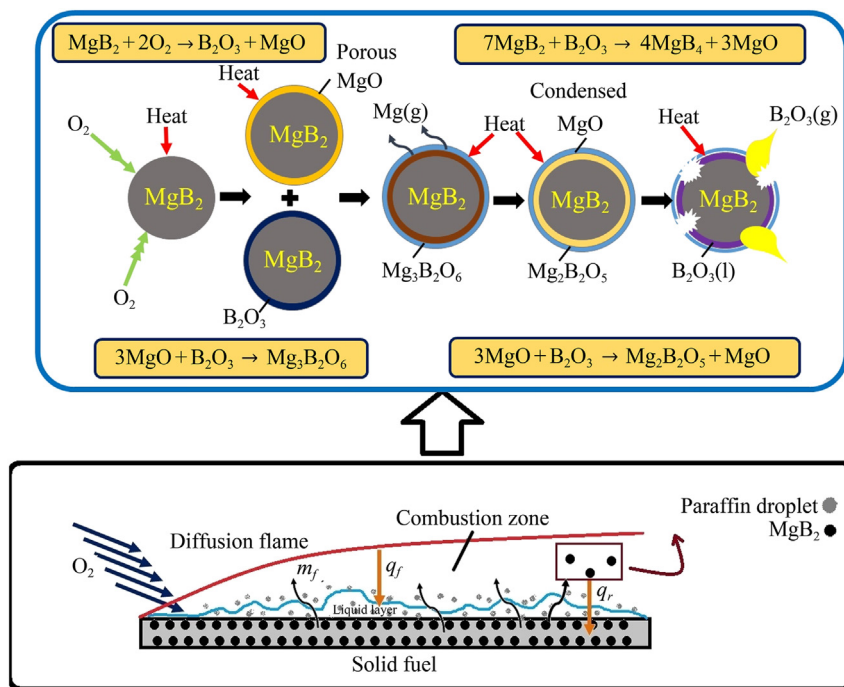


**Figure 14** Combustion mechanism of  $\text{MgB}_2$  loaded in paraffin matrix.

that due to the acceleration of the oxidation process at high temperatures (1573 K), the  $\text{MgB}_4$  phase formed in step II is converted into the  $\text{MgB}_7$  phase. The existence of  $\text{Mg}_2\text{B}_2\text{O}_5$  phases in step III could be due to the melting of the  $\text{Mg}_3\text{B}_2\text{O}_6$  phase formed in step II [46]. Also, as the temperature increases, the diffusion pathways in the oxide layer are destroyed due to the phase transition, which ultimately results in weight gain in step III (Figure 11). The surface morphology of the residues of step III was completely changed compared to that of step II (Figure 13(d)). It can be seen that the combustion residues consist of some irregular clusters with agglomeration, and the sizes of the clusters are mainly ranging to several nanometers, which are considerably smaller than the residues of step II. The phase morphology and compositions by scanning a small surface of combustion residues at higher magnification using SEM-EDS (Figure 13(e)) were further confirmed. The EDS measurement confirmed the existence of a condensed  $\text{MgO}$  oxide layer in the residues of step III. The  $\text{Mg}_3\text{B}_2\text{O}_6$  phases in step II could be decomposed into  $\text{Mg}_2\text{B}_2\text{O}_5$  and  $\text{MgO}$  at around 1523 K, and after the cooling process of the furnace, the condensed  $\text{MgO}$  oxide layer was deposited on the residue. In step IV, the weight gain rate was decreased to about 1.3%, which could be due to the condensed  $\text{MgO}$  oxide layer formed in step III and barricading the further oxidation process. Based on the above results, a combustion model of  $\text{MgB}_2$  in the paraffin matrix was proposed (Figure 14). During combustion, paraffin fuel develops a liquid layer on the fuel surface [13]. When an oxidiser stream flows over a thin, low-viscosity liquid layer, unstable waves form on the liquid surface, with tiny paraffin droplets rolling up at the edge of the surface. These droplets are entrained with  $\text{MgB}_2$

particles and burned with oxidiser flow in the combustion zone. The low-viscosity and unstable liquid layer promote the additional mass transfer to the combustion zone by entraining liquid droplets [12]. The presence of  $\text{MgB}_2$  particles in the combustion zone can increase radiative heat transfer, the heat of oxidation, and adiabatic flame temperature, which can ultimately enhance the specific impulse of a hybrid rocket.  $\text{MgB}_2$  can increase the regression rate by releasing significant energy during oxidation. Several studies reported that adding metallic additives such as Al, B, and  $\text{LiAlH}_4$  in the fuel grain does not significantly improve the regression rate [10,45,51,52]. The formation of a protective oxide layer during the oxidation of these metallic additives can impede the benefit of radiative heat transfer flux in the combustion zone. In this study, the oxidation of  $\text{MgB}_2$  allowed easier diffusion of Mg vapors to the combustion zone. During the initial stage of combustion, the oxygen vapor diffuses towards the  $\text{MgB}_2$  and the melting of elemental Mg takes place around 923 K. Further raising the temperature, the Mg can be easily oxidised and release a large amount of heat energy.

The oxidation of  $\text{MgB}_2$  starts at around 1223 K–1273 K with the formation of a liquid layer of Mg around the core  $\text{MgB}_2$  particle. The deposition of a non-protective Mg oxide layer can support diffusion pathways along grain boundaries and release a significant amount of heat in the combustion zone [53]. At high temperatures, the rapid oxidation of  $\text{MgB}_2$  occurred, which produced  $\text{MgB}_4$  and  $\text{Mg}_2\text{B}_2\text{O}_5$  phases. As the temperature further increased during the combustion process, the  $\text{MgB}_4$  phase transformed to  $\text{MgB}_7$  whereas,  $\text{Mg}_3\text{B}_2\text{O}_6$  phases were produced due to the melting of  $\text{Mg}_2\text{B}_2\text{O}_5$ . The core  $\text{MgB}_x$  is expected to burn at a higher

temperature after the non-protective liquid oxide layer evaporates (Figure 13(g)). After exposure to the oxidiser, core  $\text{MgB}_x$  particles burn and release a large amount of radiation energy to the fuel surface. Therefore, the combustion of  $\text{MgB}_2$  could improve the combustion performance of hybrid/ramjet engines when burning in oxygen/air environments.

#### 4. Conclusions

In this study, the paraffin fuel loaded with CB and  $\text{MgB}_2$  additives was manufactured with the melt cast technique. The mechanical, thermal and ballistic performance was evaluated to rate the  $\text{MgB}_2$  as a potential energetic additive for hybrid rocket applications. Some unique observations can be drawn below:

- Mechanical performance results showed that adding nano-sized  $\text{MgB}_2$  improved the ultimate strength and elastic modulus, whereas adding micro-sized CB additive into paraffin did not significantly improve. Adding these fillers exhibited a strong interaction in the wax matrix and improved the hardness of paraffin-based fuel.
- The low-temperature decomposition, melting enthalpy, and thermal energy transfer mechanism associated with these additives-loaded paraffin fuels were superior to pure paraffin. The thermal stability of the paraffin matrix was slightly improved with the addition of the CB additive.
- When the CB and  $\text{MgB}_2$  were added to paraffin, the average regression rates increased by 32% and 52%, respectively, over unmodified paraffin wax. The high regression rates associated with  $\text{MgB}_2$  are attributed to an increased heat flux caused by the oxidation of  $\text{MgB}_2$ . This was confirmed with the oxidation furnace tests performed at the temperature range of 1133 K–1603 K.
- The measured characteristic velocity efficiency of tested fuels was found in the range of 68%–79% at an O/F ratio of 1.5–2.6, which is comparable to that of practical application in a hybrid rocket.
- Finally, a combustion model of  $\text{MgB}_2$  in the paraffin matrix, which displayed various oxidation processes, was proposed. The diffusion of Mg vapors could prevent the formation of a closed oxide layer and allow easier oxidation of core particles. The high combustion efficiency associated with  $\text{MgB}_2$  fuels could be attributed to the vapor phase combustion of Mg.

These mechanical, thermal, and ballistic results are vital for accurately predicting the performance characteristics of the particular propellant combination and hence will assist in developing a low-altitude hybrid rocket system. Further, the  $\text{MgB}_2$  combustion model in the paraffin matrix will allow for accurate and efficient predictions of various oxidation processes for many combustion situations of practical relevance.

#### Acknowledgements

The authors gratefully acknowledge the Hindustan Institute of Technology and Science for their support and experimental facilities. Additionally, the authors thank the Centre for Clean Energy and Nano Convergence (CEN-CON), for providing the Nabertherm furnace facilities.

#### References

- [1] A. Narune, E. Prasad, Global Small Satellite Market Opportunity Analysis and Industry Forecast, 2019-2026, US, 2019, <https://www.nsr.com/research/global-satellite-manufacturing-and-launch-markets-10th-edition/>. (Accessed 6 May 2021).
- [2] A. Mazzetti, L. Merotto, G. Pinarello, Paraffin-based hybrid rocket engines applications: a review and a market perspective, *Acta Astronaut.* 126 (2016) 286–297.
- [3] E. Paccagnella, F. Barato, D. Pavarin, A. Karabeyoglu, Scaling parameters of swirling oxidizer injection in hybrid rocket motors, *J. Propul. Power* 33 (6) (2017) 1378–1394.
- [4] M. Kobald, C. Schmierer, H.K. Ciezki, S. Schlechtriem, E. Toson, L.T. De Luca, Viscosity and regression rate of liquefying hybrid rocket fuels, *J. Propul. Power* 35 (5) (2017) 1245–1251.
- [5] M.A. Karabeyoglu, G.G. Zilliac, B.J. Cantwell, S. De Zilwa, P. Castellucci, Scale-up Tests of High Regression Rate Liquefying Hybrid Rocket Fuels, 2003, AIAA-2003-1162, <https://doi.org/10.2514/6.2003-1162>.
- [6] B. Ahn, H. Kang, E. Lee, Y. Yun, S. Kwon, Design of multiport grain with hydrogen peroxide hybrid rocket, *J. Propul. Power* 34 (5) (2018) 1189–1197.
- [7] C. Lee, Y. Na, J.W. Lee, Y.H. Byun, Effect of induced swirl flow on regression rate of hybrid rocket fuel by helical grain configuration, *Propellant Combust. Phenom.* 11 (1) (2007) 68–76.
- [8] Y.J. Kim, C.H. Sohn, M. Hong, S.Y. Lee, An analysis of fuel-oxidiser mixing and combustion induced by swirl coaxial jet injector with a model of gas-gas injection, *Aero. Sci. Technol.* 37 (2014) 37–47.
- [9] A. Sossi, E. Duranti, M. Manzoni, C. Paravan, L.T. DeLuca, A.B. Vorozhtsov, M.I. Lerner, N.G. Rodkevich, A.A. Gromov, N. Savin, Combustion of HTPB-Based solid fuels loaded with coated nanoaluminum, *Combust. Sci. Technol.* 185 (2013) 17–36.
- [10] S.A. Hashim, S. Karmakar, A. Roy, S.K. Srivastava, Regression rates and burning characteristics of boron-loaded paraffin-wax solid fuels in ducted rocket applications, *Combust. Flame* 191 (2018) 287–297.
- [11] S. Elanjickal, A. Gany, Enhancement of the fuel regression rate in hybrid propulsion by expandable graphite additive, *Combust. Sci. Technol.* 192 (2020) 1253–1273.
- [12] M.A. Karabeyoglu, D. Altman, B.J. Cantwell, Combustion of liquefying hybrid propellants, part 1: general theory, *J. Propul. Power* 18 (3) (2002) 610–620.
- [13] M.A. Karabeyoglu, B.J. Cantwell, Combustion of liquefying hybrid propellants, part 2: stability of liquid films, *J. Propul. Power* 18 (3) (2002) 621–630.
- [14] Y. Tang, S. Chen, W. Zhang, R. Shen, L.T. DeLuca, Y. Ye, Mechanical modifications of paraffin-based fuels and the effects on combustion performance, *Propellants, Explos. Pyrotech.* 42 (2017) 1268–1277.
- [15] J. DeSain, B. Brady, K. Metzler, T. Curtiss, T. Albright, Tensile tests of paraffin wax for hybrid rocket fuel grains, in: 45th AIAA/ASME/SAE/ASEE Joint Propulsion Conference & Exhibit, Denver, Colorado, 2009, AIAA-2009-5115, <https://doi.org/10.2514/6.2009-5115>.
- [16] S. Kim, H. Moon, J. Kim, J. Cho, Evaluation of paraffin-polyethylene blends as novel solid fuel for hybrid rockets, *J. Propul. Power* 31 (6) (2015) 1750–1760.

- [17] R. Kumar, P.A. Ramakrishna, Studies on EVA-based wax fuel for launch vehicle applications, *Propellants, Explos. Pyrotech.* 41 (2) (2016) 295–303.
- [18] K. Veale, S. Adali, J. Pitot, M. Brooks, A review of the performance and structural considerations of paraffin wax hybrid rocket fuels with additives, *Acta Astronaut.* 141 (2017) 196–208.
- [19] Y. Pal, K.H. Kumar, Y.H. Li, Ballistic and mechanical characteristics of paraffin-based solid fuels, *CEAS Space J* 11 (3) (2019) 317–327.
- [20] K. Veale, S. Adali, J. Pitot, C. Bemont, The structural properties of paraffin wax based hybrid rocket fuels with aluminium particles, *Acta Astronaut.* 151 (2018) 864–873.
- [21] A. Gany, D.W. Netzer, Fuel performance evaluation for the solid-fueled ramjet, *Int. J. Turbo Jet Engines* 2 (2) (1985) 157–168.
- [22] Y. Guo, W. Zhang, X. Zhou, T. Bao, Magnesium boride sintered as high-energy fuel, *J. Therm. Anal. Calorim.* 113 (2) (2013) 787–791.
- [23] A.E. De Morais Bertoldi, M. Bouziane, P. Hendrick, C. Vande Valde, M. Lefebvre, C.A.G. Veras, Development and test of magnesium-based additive for hybrid rockets fuels, in: 2018 SpaceOps Conf. American Institute of Aeronautics and Astronautics, Marseille, France, 2018, AIAA 2018-2383, <https://doi.org/10.2514/6.2018-2383>.
- [24] S.N. Mahottamananda, N.P. Kadiresh, Y. Pal, Regression rate characterization of HTPB-paraffin based solid fuels for hybrid rocket, *Propellants, Explos. Pyrotech.* 45 (11) (2020) 1755–1763.
- [25] J.W. Gooch, *Astm D638*, in: J.W. Gooch (Ed.), *Encycl. Dict. Polym.*, Springer New York, New York, NY, 2011, p. 51, [https://doi.org/10.1007/978-1-4419-6247-8\\_856](https://doi.org/10.1007/978-1-4419-6247-8_856).
- [26] ASTM D1321-10-standard test method for needle penetration of petroleum waxes, in: *Encycl. Dict. Polym.*, Springer, New York, NY, 2010, pp. 1–20, [https://doi.org/10.1007/978-1-4419-6247-8\\_856](https://doi.org/10.1007/978-1-4419-6247-8_856).
- [27] M.A. Karabeyoglu, D. Altman, B.J. Cantwell, Development and testing of paraffin-based hybrid rocket fuels, in: 37th AIAA/ASME/SAE/ASEE Joint Propulsion Conference & Exhibit, American Institute of Aeronautics and Astronautics, 2001, AIAA-2001-4503.
- [28] G.P. Santos, S.M. Pedreira, P.T. Lacava, Physical property and carbon black distribution impact on propulsion efficiency of paraffin-based fuel, in: *Adv. Aerosp. Technol.*, American Society of Mechanical Engineers (ASME), Houston, Texas, USA, 2012, pp. 529–541, <https://doi.org/10.1115/IMECE2012-89201>.
- [29] S. Ryu, S. Han, J. Kim, H. Moon, J. Kim, S.W. Ko, Tensile and compressive strength characteristics of aluminized paraffin wax fuel for various particle size and contents, *J. Korean Soc. Propuls. Eng.* 20 (5) (2016) 70–76.
- [30] J.A. Molefi, A.S. Luyt, I. Krupa, Comparison of the influence of Cu micro- and nano-particles on the thermal properties of polyethylene/Cu composites, *Express Polym. Lett.* 3 (10) (2009) 639–649.
- [31] B.F. Yousif, K.O. Low, C.M. Tan, K.H. Oi, K.L. Ong, K.L. Ng, On the effect of carbon black on mechanical properties of recycled LDPE, HDPE and PP, in: *Proceedings of Conference on Manufacturing and Electronic Technology (COMET)*, Johor, Malaysia, 2006, pp. 15–18.
- [32] I. Islam, S. Sultana, S. Kumer Ray, H. Parvin Nur, Md. Hossain, W. Md. Ajmotgir, Electrical and tensile properties of carbon black reinforced polyvinyl chloride conductive composites, *C J* 4 (1) (2018) 15, <https://doi.org/10.3390/c4010015>.
- [33] K. Sasikumar, N.R. Manoj, T. Mukundan, M. Rahaman, D. Khastgir, Mechanical properties of carbon-containing polymer composites, in: M. Rahaman, D. Khastgir, A.K. Aldalbahi (Eds.), *Carbon-Contain. Polym. Compos.*, Springer Singapore, Singapore, 2019, pp. 125–157, [https://doi.org/10.1007/978-981-13-2688-2\\_4](https://doi.org/10.1007/978-981-13-2688-2_4).
- [34] B. Su, Y.G. Zhou, H.H. Wu, Influence of mechanical properties of polypropylene/low-density polyethylene nanocomposites: compatibility and crystallisation, *Nanomater. Nanotechnol.* 7 (2017), <https://doi.org/10.1177/1847980417715929>.
- [35] Y. Wang, C. Yang, Y. Cheng, Y. Zhang, A molecular dynamics study on thermal and mechanical properties of graphene-paraffin nanocomposites, *RSC Adv.* 5 (101) (2015) 82638–82644.
- [36] P. Zapata, H. Palza, B. Diaz, A. Armijo, F. Sepúlveda, J. Ortiz, M. Ramirez, C. Oyarzún, Effect of CaCO<sub>3</sub> nanoparticles on the mechanical and photo-degradation properties of LDPE, *Molecules* 24 (1) (2018) 126.
- [37] D.S. Maki, N.K. Nemer, S.M. Uosof, S.N. Mohi, Use of nano chemical additives to improve the properties of industrial used paraffin wax, *Iraqi J. Sci.* (2019) 99–104.
- [38] P. Cristina Gomes Fernandes, J. Santos Gomes, E. Yoshie Kawachi, M. Yuji Nagamachi, L. Fernando de Araujo F Ferrão, K. Pereira Cardoso, Exploring the Mechanical, Thermal and ballistic effects of carbon black on paraffin-based fuels for hybrid rocket motors, *J. Aero. Technol. Manag.* (2020) 19–22, <https://doi.org/10.5028/jatm.etmq.64>.
- [39] J. Clarke, J.F. Harper, D.M. Price, J. Zhang, Effect of carbon black grade on the microwave heating of high-density polyethylene, *J. Appl. Polym. Sci.* 31 (2007) 1–9.
- [40] A.S. Luyt, J.A. Molefi, H. Krump, Thermal, mechanical and electrical properties of copper powder filled low-density and linear low-density polyethylene composites, *Polym. Degrad. Stabil.* 91 (7) (2006) 1629–1636.
- [41] J.C. Thomas, C. Paravan, J.M. Stahl, A.J. Tykol, F.A. Rodriguez, L. Galfetti, E.L. Petersen, Experimental evaluation of HTPB/paraffin fuel blends for hybrid rocket applications, *Combust. Flame* 229 (2021) 111386.
- [42] C. Mandilas, G. Karagiannakis, A.G. Konstandopoulos, C. Beatrice, M. Lazzaro, G. Di Blasio, S. Molina, J.V. Pastor, A. Gil, Study of oxidation and combustion characteristics of iron nanoparticles under idealized and engine like conditions, *Energy Fuels* 30 (2016) 4318–4330.
- [43] J.R. Taylor, *Introduction to Error Analysis: the Study of Uncertainties in Physical Measurements*, second ed., University Science Books, Sausalito, 1997.
- [44] S. Kim, H. Moon, J. Kim, Thermal characterisations of the paraffin wax/low density polyethylene blends as a solid fuel, *Thermochim. Acta* 613 (2015) 9–16.
- [45] C. Carmicino, F. Scaramuzzino, A. Russo Sorge, Trade-off between paraffin-based and aluminium-loaded HTPB fuels to improve performance of hybrid rocket fed with N<sub>2</sub>O, *Aero. Sci. Technol.* 37 (2014) 81–92.
- [46] Y. Guo, W. Zhang, D. Yang, R.-L. Yao, Decomposition and oxidation of magnesium diboride, *J. Am. Ceram. Soc.* 95 (2) (2012) 754–759.
- [47] E. Aksu, Study of MgB<sub>2</sub> phase formation by using XRD, SEM, thermal and magnetic measurements, *J. Alloys Compd.* 552 (2013) 376–381.
- [48] M.J. Chiverini, N. Serin, D.K. Johnson, Y.C. Lu, K.K. Kuo, G.A. Risha, Regression rate behavior of hybrid rocket solid fuels, *J. Propul. Power* 16 (1) (2000) 125–132.
- [49] S. Gordon, B.J. McBride, *Computer Program for Calculation of Complex Chemical Equilibrium Compositions and Applications, Part 1: Analysis*, United States, 1994, pp. 1–61, <https://ntrs.nasa.gov/citations/19950013764>.
- [50] H. Karakas, O. Kara, I. Ozkol, A.M. Karabeyoglu, Performance enhancing additives for hybrid rockets, in: AIAA Propulsion and Energy 2019 Forum, American Institute of Aeronautics and Astronautics, Indianapolis, 2019, <https://doi.org/10.2514/6.2019-3922>.
- [51] B. Evans, N.A. Favorito, E. Boyer, Characterization of solid fuel mass-burning enhancement utilising an X-ray translucent hybrid rocket motor, *Int. J. Energ. Mater. Chem. Propuls.* 6 (6) (2007) 713–732.
- [52] D.B. Larson, J.D. Desain, E. Boyer, T. Wachs, K.K. Kuo, R. Borduin, J.H. Koo, B. Brady, T.J. Curtiss, G. Story, Formulation, casting, and evaluation of paraffin-based solid fuels containing energetic and novel additives for hybrid rockets, *Int. J. Energ. Mater. Chem. Propuls.* 14 (6) (2015) 453–478.
- [53] L. Liu, P. Liu, G. He, Ignition and combustion characteristics of compound of magnesium and boron, *J. Therm. Anal. Calorim.* 121 (2015) 1205–1212.